Int J Disaster Risk Sci (2022) 13:275–290
https://doi.org/10.1007/s13753-022-00407-4

www.ijdrs.com
www.springer.com/13753

ARTICLE

Risk Assessment of Tsunamis Along the Chinese Coast Due to Earthquakes

Chun Hui[1,2,3] · **Lixin Ning**[1,2,3] · **Changxiu Cheng**[1,2,3,4]

Accepted: 17 February 2022 / Published online: 1 April 2022

Abstract China's coastal areas are densely populated, economically developed, and located in close proximity to several potential tsunami sources; therefore, tsunami risk cannot be ignored. This study assessed tsunami risk in coastal areas of China by developing a framework for tsunami risk assessment from the perspectives of hazards, vulnerability, and exposure. First, a probabilistic tsunami hazard assessment (PTHA) model was applied to estimate the potential tsunami sources in both local crustal faults and circum-Pacific subduction zones based on numerical simulations. The output of the PTHA includes tsunami wave height distributions along the coast. Then, an indicator system reflecting exposure and vulnerability to tsunamis in the coastal areas of China was established by using the entropy method and analytic hierarchy process. The PTHA findings show that the tsunami wave height is close to 3 m on the southern coast of the Bohai Sea, the Pearl River Estuary, and the Yangtze River Delta and exceeds 2 m near the Taiwan Strait for the 2000-year return period. The results of the tsunami risk assessment show that the cities at the highest risk level (level I) include Tangshan, Yantai, and Hong Kong, while cities at the high risk level (level II) include Fuzhou, Xiamen, and Quanzhou near the Taiwan Strait and many cities on the Yangtze River Delta, the Pearl River Estuary, and the southern coast of the Bohai Sea. Our findings can provide an understanding of differences in tsunami risk between Chinese coastal cities that may be affected by tsunamis in the future.

Keywords China coast · Earthquakes · Probabilistic tsunami hazard assessment · Tsunami exposure · Tsunami risk · Vulnerability

1 Introduction

Tsunamis are one of the most serious disasters that pose a high risk in many coastal countries and regions. Although tsunamis can be induced by many causes, such as earthquakes, submarine landslides, volcanic eruptions, and meteorite impacts (Smit et al. 2017), the global historical record shows that approximately 80% of tsunamis are generated by earthquakes (Løvholt et al. 2014; Shen et al. 2018; Ning et al. 2021). Japan's National Disaster Management Agency (BNPB) defines a tsunami as a series of large sea waves arising due to shifts in the seabed caused by earthquakes. Tsunami intensity is highly correlated with the earthquake magnitude, depth, and rupture process (Ambraseys and Synolakis 2010). Recent large tsunami events in Sumatra (2004), Japan (2011), and Chile (2010, 2015) following major earthquakes have caused catastrophic damage and many deaths or missing persons. Thus, most current studies that have assessed future tsunami risk have focused on tsunamis caused by earthquakes. China is a large country with a mainland coastline of 18,000 km, and local crustal faults and subduction faults have been identified along the coast. These faults have the potential to

✉ Changxiu Cheng
chengcx@bnu.edu.cn

[1] Key Laboratory of Environmental Change and Natural Disaster, Beijing Normal University, Beijing 100875, China

[2] State Key Laboratory of Earth Surface Processes and Resource Ecology, Beijing Normal University, Beijing 100875, China

[3] Faculty of Geographical Science, Beijing Normal University, Beijing 100875, China

[4] National Tibetan Plateau Data Center, Beijing 100101, China

trigger large earthquakes; therefore, the tsunami threat to coastal cities is serious (Ren et al. 2014, Ren et al. 2017; Yuan et al. 2021).

According to the regional disaster system theory (Shi 1996), investigations of tsunami risk from an integrated perspective are increasingly warranted, and they should consider tsunami hazards (wave height, inundated area, flow depth, flow velocity, and so on) as well as factors associated with exposure and vulnerability (people, socioeconomic systems, infrastructure, and so on) to tsunamis. Quantifying the exposure and vulnerability of all factors in the area is challenging, and researchers usually select representative indicators, including demographic and economic, for analysis (Cong et al. 2019). In contrast, tsunami hazard assessment methods are well developed, and two main approaches have been applied in tsunami hazard analysis: (1) the scenario approach; and (2) probabilistic tsunami hazard assessment (PTHA). In the scenario approach, the dynamic processes of tsunami generation with credible parameters are modeled to produce maps depicting tsunami wave height and inundation footprint. The earthquake scenarios developed using the scenario approach are most often confined to situations where tsunamis may be generated due to seismic dip–slip motion (Løvholt et al. 2014). Researchers usually focus on the worst-case tsunami scenario to assess the deterministic tsunami hazard by modeling the offshore wave height (Lorito et al. 2008; Harbitz et al. 2012). This approach can provide valuable information to minimize the effects of tsunamis on certain coastal projects and structures; however, the disadvantages of this method are that the results rarely emphasize the possibility of these events occurring and are highly sensitive to the selected scenario parameters, for example, the moment magnitude of earthquakes, the width and length of faults (Shaw et al. 2008; Wijetunge 2014). In contrast, PTHA is relatively complex because it considers all possible tsunami events in order to estimate the probability of a wave height at a particular location above a threshold level over a period of time (Geist and Parsons 2006; Parsons and Geist 2008). The PTHA approach is advantageous because it provides a determined likelihood of occurrence and return periods, which are essential for engineering design, risk mitigation, land-use planning, and insurance, but the uncertainties in the simulation are difficult to quantify (Grezio et al. 2017; Mori et al. 2018). Previous studies have extended the application of PTHA to many coastal countries and regions, such as New Zealand (Power et al. 2013), Japan (De Risi et al. 2017), the US (Omira et al. 2015), the Pacific coast (Smit et al. 2017; Zamora and Babeyko 2020), and the South China Sea (Ren et al. 2017; Yuan et al. 2021).

A series of survey projects and studies in China have been conducted to investigate potential disaster events such as earthquakes and tsunamis in China's seas and adjacent areas. Tsunamis have been documented in China and have caused disasters in Taiwan (Liu et al. 2007). Zhou and Adams (1988) first proposed a zoning map of the tsunami hazard along China's coast based on the geology and earthquake characteristics of the continental shelf. Wu and Huang (2009) conducted a numerical simulation of tsunamis in Taiwan and focused on the threat posed by the Manila Trench, which is 100 km away from Taiwan. Ren et al. (2009) analyzed the sensitivity of the earthquake magnitude effect of a potential tsunami source on the tsunami wave amplitude on Taiwan Island. Hou et al. (2016) simulated the probable maximum tsunami amplitude and tsunami arrival time along the coast of China's mainland from tsunami sources in Taiwan, and the results show that Guangdong, Fujian, and parts of Zhejiang are the areas with the highest hazard level. Feng et al. (2017) adopted the numerical simulation method to assess tsunami hazards in coastal areas of Shandong Province, eastern China. Moreover, PTHA studies have focused more on the South China Sea coast in China's mainland, where eight local crustal faults have been recognized as potential tsunami sources (Ren et al. 2017), and the Manila Trench has been identified as the source region with the highest tsunami hazard (Li et al. 2016). Yuan et al. (2021) considered both the local crustal faults on the continental shelves and the faults around the circum-Pacific subduction zones when applying the PTHA method to the coast of the South China Sea. Xie et al. (2020) compiled and analyzed the completeness of earthquake catalogs for China's seas and adjacent regions and provided valuable information on the tsunami risk along the Chinese coast caused by tsunamigenic earthquakes.

Although previous works have focused mostly on tsunami hazard assessments (Ren et al. 2014; Ren et al. 2017; Batzakis et al. 2020; Yuan et al. 2021), exposure and vulnerability assessments also must be performed for coastal risk planning and management. Our study integrated tsunami hazard information and indicators on the associated exposure and vulnerability. Specifically, we applied the PTHA method to all potential tsunami sources (local crustal sources and circum-Pacific subduction zones). Then composite indices of exposure and vulnerability were adopted for coastal cities in China (except Taiwan), and indicators related to exposure and vulnerability were selected to calculate the indices. After analyzing the hazard, vulnerability, and exposure, we identified the tsunami risk levels of coastal cities.

2 Conceptual Tsunami Risk Assessment Framework

The tsunami risk assessment method used in the present study builds on the classic risk assessment approach proposed by the United Nations Office for Disaster Risk Reduction (UNISDR) and the Intergovernmental Panel on Climate Change (IPCC) as developed by Field et al. (2014) and UNISDR (2019), which state that risk is a function of hazard, exposure, and vulnerability. Figure 1 shows the overall workflow of the assessment. Hazards are described as events that cause a severe disturbance in the water mass, provide high energy, and result in enormous waves (Witter et al. 2003; Batzakis et al. 2020). From a tsunami wave perspective, hazard assessment builds on the PTHA method, which quantifies the wave height distribution along the coast corresponding to a given return period. With the PTHA, statistical analyses can be applied in particular regions where historical records of tsunamigenic earthquakes are available. In areas where these historical records are scarce, synthetic seismic catalogs are usually generated using the Monte Carlo technique. We built a database of tsunami numerical simulations for the following variables: faults, earthquake magnitudes and their locations, depths, and frequencies. From this database, we generated a series of wave height distributions and mapped the maximum values for the return periods of 200, 500, 1000, and 2000 years. Frischen et al. (2020), in addressing drought risk in Zimbabwe, define exposure as the presence of people, plants and animals, properties, and assets in places that could be affected by a hazard, a definition that would apply equally well to tsunamis. Similarly, when Ortega-Gaucin et al. (2021) assessing an agricultural drought risk in Zacatecas, Mexico, vulnerability was defined as the sensitivity and fragility of systems affected by a hazard and the potential capacity of local socioeconomic systems, and this definition is also applicable to tsunamis.

Modeling the exposure and vulnerability of people or assets is difficult due to the large diversity and different data availability of households, economies, and buildings. In the present study, we adopted composite indices for China's coastal cities by integrating indicators identified in previous studies and considering data validity and availability (Thorn et al. 2015; Zhang et al. 2019). The method consists of choosing indicators, searching data that are highly relevant to the indicators, applying statistical treatment to generate weights for the indicators, and then assigning coefficients to the indicators and combining them into maps of exposure and vulnerability. Specifically, exposure includes variables related to population and economic characteristics, such as population density and gross domestic product (GDP) (Dewan 2013; Batzakis et al. 2020). Vulnerability indicators are related to resilience and adaptation characteristics, such as the mainland coastline length, proportion of social security personnel (health workers, police force, community staff, and so on), proportion of science and technology expenditure, per capita GDP, and elevation (Wang et al. 2020; Ye et al. 2020).

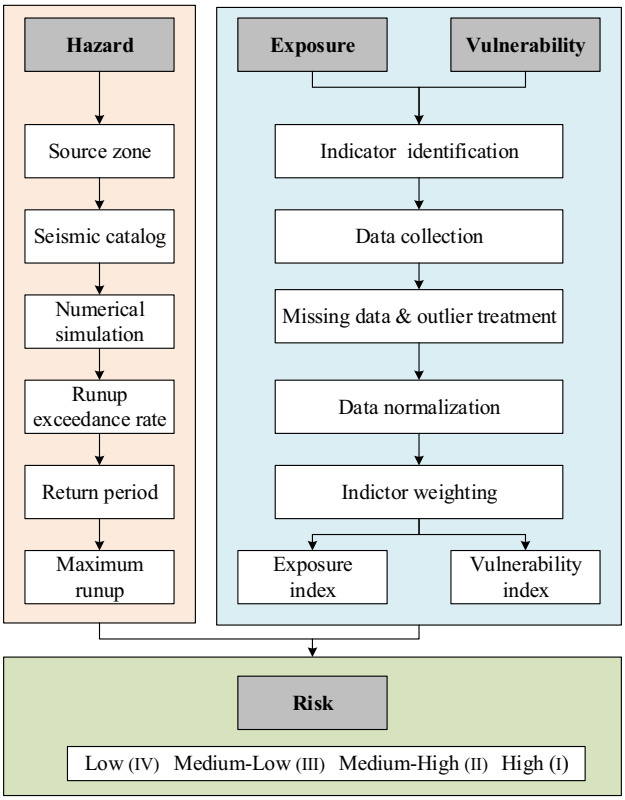

Fig. 1 Workflow for tsunami risk assessment of coastal cities in China

Multiple types of data were obtained, including spatial data, statistical data, and analog data. A statistical analysis, which includes missing data and outlier processing, and multicollinearity analysis, was then performed. The wave heights of all hazard points in the coastal area of each city were identified, and the maximum wave height was selected as the hazard intensity of the city. Data for indicators of exposure and vulnerability were collected and analyzed on a city-level basis. As a final step, the results for city-level hazard, exposure, and vulnerability to tsunamis are integrated to determine the level of potential risk.

3 Materials and Methods

Potential tsunami sources (local crustal sources and circum-Pacific subduction zones) along the Chinese coasts are presented in Sect. 3.1. The steps of the PTHA are given in Sect. 3.2. Exposure and vulnerability assessment is

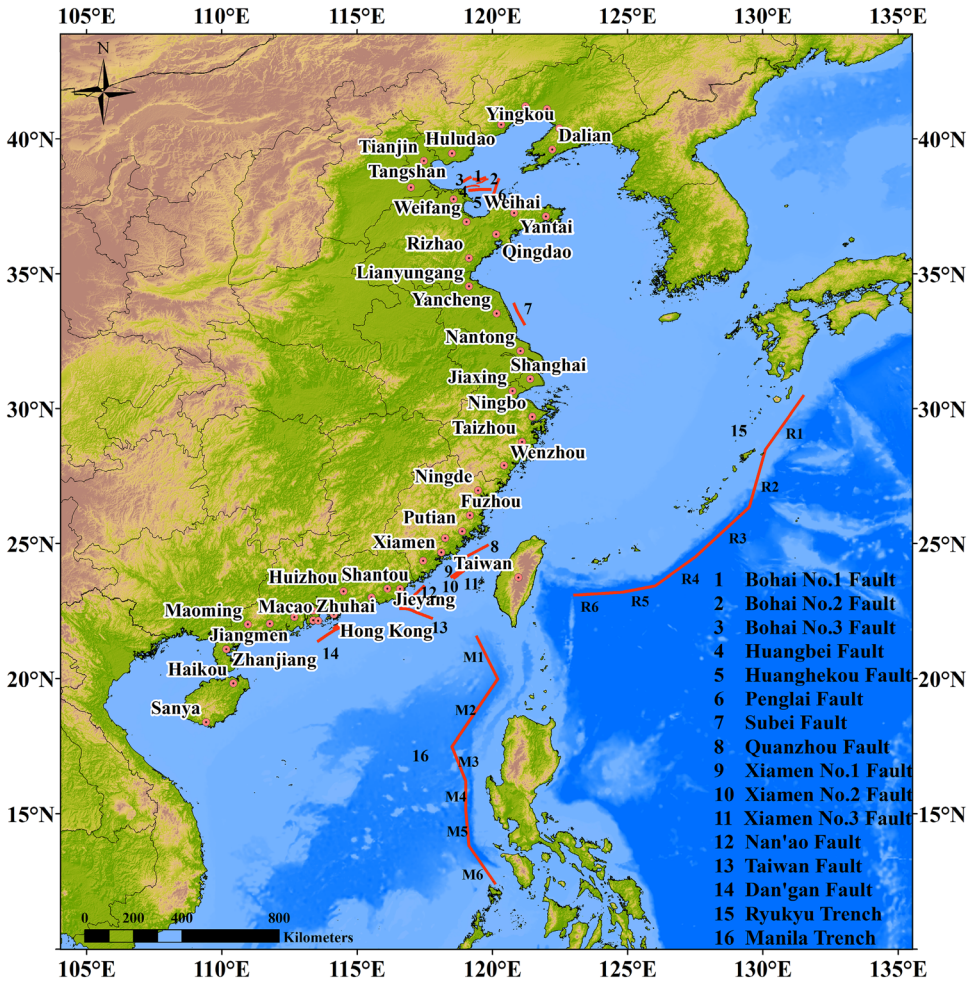

Fig. 2 Distribution of faults identified as potential tsunami sources of the coastal region of China. R1–6 are tectonic segments of the Ryukyu Trench and M1–6 are tectonic segments of the Manila Trench

presented in Sect. 3.3, and the assessment scheme of tsunami risk levels for China's coastal cities is presented in Sect. 3.4.

3.1 Study Area

The coastal region of China lies on the southeastern edge of Eurasia, with a coastline of 18,000 km. These coastal areas include China's important political, economic, cultural, and scientific and technological centers. The region has dozens of megacities and a dense and unevenly distributed population, and has experienced rapid economic development in recent decades. Moreover, the region is threatened by tsunamis due to nearby potential tsunami sources, which include both faults around the circum-Pacific subduction zones, such as the Ryukyu Trench and Manila Trench, and local crustal faults on the continental shelves (Fig. 2). Two large crustal faults—the Tanlu fault and the Yanshan-Bohai fault—are located in the Bohai Sea, along which almost all large earthquakes recorded in China have occurred (Shi et al. 2012; Wang et al. 2014). The Subei fault zone in the Yellow Sea and the Ryukyu Trench, at the northwestern boundary of the Pacific, have been regarded as potential seismic sources that could induce severe tsunamis along the eastern coast of China (Ren et al. 2017). The South China Sea is located at the junction of the Eurasian, Pacific, and Australian plates, which are associated with high seismicity, and is surrounded by the Manila Trench and eight local potential tsunami sources (Liu et al. 2009; Ren et al. 2014).

3.2 Tsunami Hazard Analysis

The exceedance rate of tsunami wave height at a set of hazard points off the coast is calculated for the PTHA, which follows the same procedure as the probabilistic seismic hazard assessment (PSHA) developed by Cornell (1968). A PTHA can be conducted in four steps: (1) identification and characterization of tsunami source zones; (2) creation of an earthquake catalog based on tsunami sources; (3) modeling of sea surface displacement and numerical propagation; and (4) distribution of the modeled wave height and calculation of the exceedance rate.

Table 1 Tectonic activity parameters of tsunami sources of China's coastal region

Fault	Strike (°)	Dip (°)	Rake (°)	Length (km)	Width (km)	Depth (km)
Bohai No. 1	229	45	90	53	71	30
Bohai No. 2	254	45	90	51	71	30
Bohai No. 3	66	60	90	35	50	30
Huangbei	86	60	90	55	71	35
Huanghekou	88	45	90	79	71	30
Penglai	23	60	90	113	71	30
Subei	148	60	90	114	50	30
Quanzhou	65	60	90	92	71	20
Xiamen No. 1	58	60	90	51	71	20
Xiamen No. 2	57	60	90	74	71	20
Xiamen No. 3	53	60	90	59	71	20
Nan'ao	47	60	90	75	50	20
Taiwan	188	60	90	130	50	20
Dan'gan	63	60	90	135	50	20
Ryukyu Trench						
R1	30	15	315	290	98	15
R2	32	19	315	256	92	20
R3	45	20	310	282	97	18
R4	53	25	310	215	83	20
R5	72	30	344	130	65	25
R6	81	35	355	170	84	25
Manila Trench						
M1	350	14	110	210	82	20
M2	29	20	110	310	109	20
M3	3	20	90	135	66	20
M4	351	20	90	140	66	20
M5	353	30	50	166	71	20
M6	308	30	50	142	66.	20

3.2.1 Tsunami Source Zones

Tsunami source zones are identified based on the parameters of faults and the estimated maximum size of an earthquake that can generate tsunamis. As shown in Fig. 2, from north to south, the potential tsunami threats to China's coastal region are posed by earthquake sources in the Bohai Sea (Li et al. 2019), the East China Sea (Xie et al. 2020), and the South China Sea (Ren et al. 2014, Ren et al. 2017). The local crustal faults in the Bohai Sea, which mainly induce shallow earthquakes with focal depth less than or equal to 70 km, have the potential to generate a maximum moment magnitude (Mw) of 8.0 (Shi et al. 2012; Wang et al. 2014). For the East China Sea, there are two potential tsunami source zones: the local crustal faults in the Yellow Sea and the Ryukyu Trench. Ren et al. (2017) identified the Subei fault zone in the Yellow Sea as a potential tsunami source and determined the fault characteristics with the possibility of generating an earthquake maximum moment magnitude of 7.5. The faults in the Ryukyu Trench have been identified as six tectonic segments, and they have the potential to generate a maximum earthquake magnitude of up to Mw 8.5 (Goto et al. 2010; Ömer and Naohiko 2019). The South China Sea is located at the junction of the Eurasian, Pacific, and Australian plates. Ren et al. (2014) identified eight local potential tsunami sources in the South Sea, and the maximum moment magnitude of the earthquake was set as 7.5. The worst-case scenarios for the Manila Trench indicate that earthquakes up to Mw 9.0 could be generated (Huang et al. 2009; Liu et al. 2009). Specific values reflecting fault parameters of tsunami sources are shown in Table 1.

3.2.2 Synthetic Earthquake Catalog

We used the Monte Carlo technique to generate 100,000-year-long synthetic earthquake catalogs for each potential seismic source. The parameters required for the synthetic catalog include time T, the Gutenberg–Richter b value, the minimum magnitude $M_{\min}$, and the maximum magnitude

M_{max}. We assumed that the occurrence time of earthquakes follows a Poisson distribution (Pan et al. 2013):

$$P(n) = \frac{(v_{m_0} \cdot T)^n \exp(-v_{m_0} \cdot T)}{n!}, \quad (1)$$

where n is the number of synthetic events in time [0, T] and v_{m_0} is the mean annual rate for events above magnitude m_0, which can be obtained from the Gutenberg–Richter relationship:

$$\log N = a - b \cdot M, \quad (2)$$

where N is the cumulative number of events above magnitude M, a describes the productivity, and b signifies the relative proportion of large and small earthquakes.

The magnitudes of events in the synthetic earthquake catalog follow the probability distribution:

$$f(M) = \frac{\beta \exp[-\beta(M - M_{min})]}{1 - \exp[-\beta(M_{max} - M)]}, M_{min} \le M \le M_{max}, \quad (3)$$

where $\beta = b \cdot \ln 10$.

3.2.3 Tsunami Occurrence Model

The Cornell multigrid coupled tsunami (COMCOT) model used in this study is capable of simulating the generation and propagation of tsunamis, and its reliability and efficiency have been widely verified (Power et al. 2013; Davies et al. 2017). The COMCOT tsunami generation model works on the basis of the Okada (1985) source model, which assumes a rectangular fault plane in an elastic half-space. The deformation of the seafloor on the fault plane is considered the sea surface displacement as long as the dislocation is much faster than the wave propagation during a tsunamigenic earthquake. To compute the deformation, several fault parameters are necessary, and they can be obtained through the following empirical equations (Papazachos et al. 2004):

$$\log L = 0.55M - 2.19, \quad (4)$$

$$\log W = 0.31M - 0.63, \quad (5)$$

where L, W, and M represent the length, width, and moment magnitude of the fault plane, respectively. The slip amount of the fault plane can be estimated using the following equations (Aki 1966):

$$\log M_0 = \mu DLW, \quad (6)$$

$$M = \frac{2}{3}\log M_0 - 10.7, \quad (7)$$

where M_0 represents the scalar moment of the earthquake, μ is the shear rigidity of the Earth's mantle (3.0×10^{10} N/m) and D is the slip amount of the fault.

To produce reliable wave height estimates, it is essential to use both linear and nonlinear shallow water equations that calculate tsunami propagation from a source zone to coastal regions. For tsunamis in the Ryukyu Trench and Manila Trench, the tsunami amplitude is much smaller than the water depth (Philip et al. 1998). In COMCOT, the topo-bathymetric grid resolution is 1 arc-min, and we applied the linear shallow water equations in spherical coordinates:

$$\frac{\partial \eta}{\partial t} + \frac{1}{R\cos\varphi}\left\{\frac{\partial P}{\partial \psi} + \frac{\partial}{\partial \varphi}(\cos\varphi Q)\right\} = -\frac{\partial h}{\partial t}, \quad (8)$$

$$\frac{\partial P}{\partial t} + \frac{gh}{R\cos\varphi}\frac{\partial \eta}{\partial \psi} - fQ = 0, \quad (9)$$

$$\frac{\partial Q}{\partial t} + \frac{gh}{R}\frac{\partial \eta}{\partial \varphi} + fP = 0, \quad (10)$$

$$f = \Omega \sin\varphi, \quad (11)$$

where η represents the water surface elevation; (P, Q) denote the volume fluxes in the X (west–east) direction and Y (south–north) direction, respectively; (φ, ψ) represent the latitude and longitude, respectively; R is the radius of the Earth; g is the gravitational acceleration; h is the water depth; f denotes the Coriolis force coefficient due to the rotation of the Earth; and Ω is the rotation rate of the Earth.

For tsunamis generated by local crustal faults on continental shelves, the tsunami amplitude is not much different, the water depth resulting in the nonlinear convective inertia force and bottom friction terms become increasingly prominent, and the linear shallow water equations are no longer valid (Philip et al. 1998). In COMCOT, the topo-bathymetric grid resolution is 1 arc-min, and we used the nonlinear shallow water equations in spherical coordinates as follows:

$$\frac{\partial \eta}{\partial t} + \frac{1}{R\cos\varphi}\left\{\frac{\partial P}{\partial \psi} + \frac{\partial}{\partial \varphi}(\cos\varphi Q)\right\} = -\frac{\partial h}{\partial t}, \quad (12)$$

$$\frac{\partial P}{\partial t} + \frac{1}{R\cos\varphi}\left\{\frac{P^2}{H}\right\} + \frac{1}{R}\frac{\partial}{\partial \varphi}\left\{\frac{PQ}{H}\right\} + \frac{gH}{R\cos\varphi}\frac{\partial \eta}{\partial \psi} - fQ + F_x = 0, \quad (13)$$

$$\frac{\partial Q}{\partial t} + \frac{1}{R\cos\varphi}\frac{\partial}{\partial \psi}\left\{\frac{PQ}{H}\right\} + \frac{1}{R}\frac{\partial}{\partial \varphi}\left\{\frac{Q^2}{H}\right\} + \frac{gH}{R}\frac{\partial \eta}{\partial \varphi} + fP + F_y = 0, \quad (14)$$

$$F_x = \frac{gn^2}{H^{7/3}} P\left(P^2 + Q^2\right)^{1/2}, \quad (15)$$

$$F_y = \frac{gn^2}{H^{7/3}} Q\left(P^2 + Q^2\right)^{1/2}, \quad (16)$$

where H is the total water depth; F_x and F_y represent the bottom friction in the X and Y directions, respectively; and n is Manning's roughness coefficient.

3.2.4 Return Period and Wave Height Exceedance Rate

We selected a total of 770 nearshore points over the 10 m isobath along the Chinese coast as hazard points, except for the Bohai Sea where the 5 m isobath was used. Then, we computed the return period and exceedance rate of the tsunami wave height for every hazard point. Empirical studies have shown that tsunami wave heights can be described by the log-normal distribution (Kaistrenko 2011; Choi et al. 2012):

$$f(h) = \frac{1}{h\sigma\sqrt{2\pi}ln10}\exp\left(-\frac{(\log h-\mu)^2}{2\sigma^2}\right), \tag{17}$$

where h is the maximum wave height for each hazard point and μ and σ represent the average value and standard deviation of the height logarithm, respectively. The probability of h caused by the ith potential source zone exceeding a threshold H at the hazard point is denoted as follows:

$$p_i(h\geq H)=\frac{v_M(M_{\min}\leq M\leq M_{\max})}{\sigma\sqrt{2\pi}ln10}\int_H^{\infty} exp\left(-\frac{(\log h-\mu)^2}{2\sigma^2}\right)\frac{dh}{h}, \tag{18}$$

where v_M ($M_{\min} \leq M \leq M_{\max}$) can be obtained from Eqs. 2 and 3. If the hazard point is affected by N potential source zones, then

$$P_N(h\geq H) = 1-\prod_{i=1}^{N}\{1-p_i(h\geq H)\}. \tag{19}$$

We assumed that the occurrence time of earthquakes in the potential source zone follows a Poisson distribution. The probability of exceedance for a time period of T years can be expressed as follows:

$$P(h\geq H, t=T) = 1-\exp\{-P_N(h\geq H)\cdot T\}. \tag{20}$$

The return period is determined as follows:

$$R(h=H) = -\frac{1}{\ln\{1-P(h\geq H)\}}. \tag{21}$$

3.3 Evaluation of Exposure and Vulnerability to Tsunamis

Measures of exposure and vulnerability can include the number of people and types of assets or other settings that could be affected by tsunamis. Here, we chose the gross population and GDP of coastal areas as exposure indicators. Vulnerability indicators include mainland coastline length, proportion of social security personnel, proportion of science and technology expenditure, per capita GDP, and elevation. The data are available from the provincial statistic yearbooks[1] and the Resource and Environment Science and Data Center.[2]

3.3.1 Normalization of Indicators

Given that the indicators are of diverse types and value ranges, we first standardized the data to convert different types of indicators into the same range (0−1). The indicators were standardized using Eq. 22 if the direction of impact of the factor on the vulnerability or exposure of the element at risk is positive. Otherwise, the indicator is standardized in accordance with Eq. 23 (Zhou et al. 2020).

$$y = \frac{x^i - x^i_{\min}}{x^i_{\max} - x^i_{\min}}, \tag{22}$$

$$y = \frac{x^i_{\max} - x^i}{x^i_{\max} - x^i_{\min}}, \tag{23}$$

where x represents the indicator value before standardization and y represents the indicator value after standardization.

3.3.2 Weighting of Indicators

The weight values of the indicators in Table 2 reflect the relative importance of different indicators in the assessment of vulnerability and exposure, with a greater weight corresponding to a greater contribution of the indicator to vulnerability or exposure, and vice versa. At present, there are three main methods of calculating indicator weights: (1) methods based on subjective cognition, such as the analytic hierarchy process or direct scoring method, which have the advantage of fully utilizing experts' experience and knowledge but have great uncertainties in the results (Nan et al. 2013); (2) methods based on objective calculation, such as the entropy weight method and standard deviation method, which have the advantage of determining the weights from the data but may yield results inconsistent with prior knowledge (Li and Jin 2012); and (3) a combination of subjective and objective methods (Huang et al. 2020). In this study, we chose a combination of subjective and objective methods. First, the objective weights of the indicators were determined by the entropy weight method, and the subjective weight of each indicator was then determined based on the analytic hierarchy process, involving 10 researchers whose research fields are

[1] https://data.cnki.net/.

[2] https://www.resdc.cn/.

Table 2 Evaluation indicator system of exposure and vulnerability to coastal tsunamis in China and indicator weights

Dimension	Indicator	Direction of impact	Comprehensive weight	Entropy method	Analytic hierarchy process
Exposure	GDP	Positive	0.410	0.418	0.402
	Population	Positive	0.199	0.194	0.203
Vulnerability	Coastline length	Positive	0.158	0.261	0.055
	Proportion of social security personnel	Negative	0.032	0.020	0.043
	Proportion of science and technology expenditure	Negative	0.091	0.055	0.127
	GDP per capita	Negative	0.059	0.019	0.099
	Average elevation	Negative	0.052	0.033	0.071

Table 3 Corresponding relationships between tsunami risk and hazard, exposure, and vulnerability

E&V (Exposure and Vulnerability)	H (Hazard)			
	Low (IV)	Medium–Low (III)	Medium–High (II)	High (I)
Low (IV)	Low risk (IV)	Low risk (IV)	Medium–Low risk (III)	Medium–Low risk (III)
Medium–Low (III)	Low risk (IV)	Medium–Low risk (III)	Medium–High risk (II)	Medium–High risk (II)
Medium–High (II)	Medium–Low risk (III)	Medium–High risk (II)	Medium–High risk (II)	High risk (I)
High (I)	Medium–Low risk (III)	Medium–High risk (II)	High risk (I)	High risk (I)

oceanic geology, disasters, and so on. Finally, the comprehensive weights were obtained by the weighted average of objective and subjective weights (Hu et al. 2019).

3.3.3 Calculation of the Exposure and Vulnerability Indices

After the weights of the indicators were obtained, the following equation was used to calculate the tsunami exposure and vulnerability indices:

$$E\&V = \sum_{i=1}^{m} w_i \times y_i, \tag{24}$$

where E is the exposure index of the region, V is the vulnerability index of the region, w_i is the weight of each indicator, and y_i denotes the value of the indicator.

3.4 Determination of Tsunami Risk

Taking hazard, exposure, and vulnerability into account, the tsunami risk can be assessed according to the following equation:

$$R = H \times E \times V, \tag{25}$$

where R is the tsunami risk, H is the hazard level, E is the exposure level, and V is the vulnerability level.

As shown in Table 3, the criteria for the classification of hazard, exposure, vulnerability, and risk were derived from the Guideline for Risk Assessment and Zoning of Tsunami Disaster (Ministry of Natural Resources 2019). The results can be presented in maps that display and distinguish the different levels of hazard, exposure, and vulnerability experienced by cities on the coast.

Specifically, hazard was divided into four categories based on the height of the tsunami waves: low hazard (IV: $h \leq 0.5$ m), medium–low hazard (III: 0.5 m $< h \leq 1.0$ m), medium–high hazard (II: 1.0 m $< h \leq 2.5$ m), and high hazard (I: $h > 2.5$ m). Class I represents the maximum tsunami intensity; class IV indicates that a tsunami will not cause a disaster. In this work, we identified the wave heights of all hazard points in the coastal area of each city and selected the maximum wave height as the hazard intensity of the city. The index $E\&V$ comprehensively reflects the exposure and vulnerability to tsunamis. The $E\&V$ index was divided into four categories: low $E\&V$ (IV: v_i $\{0.6 \times N \leq i\}$), medium–low $E\&V$ (III: v_i $\{0.3 \times N < i \leq 0.6 \times N\}$), medium–high $E\&V$ (II: v_i $\{0.1 \times N < i \leq 0.3 \times N\}$), and high $E\&V$ (I: v_i $\{i \leq 0.1 \times N\}$). v_i was calculated by Eq. 24 to obtain $E\&V$ of each city ($i = 1, N$). Class I represents the high exposure and vulnerability to tsunamis; class IV indicates the least exposure and vulnerability to tsunamis.

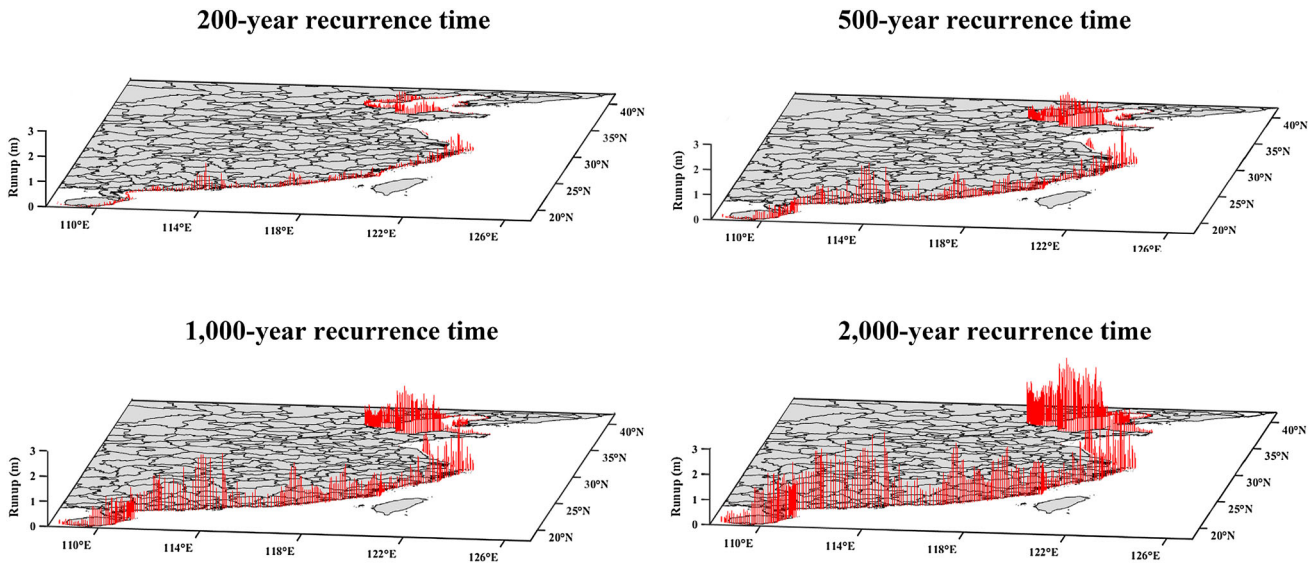

Fig. 3 Maximum tsunami wave height distribution of China's coastal region for different return periods

4 Results

In this section, we present the results obtained from the modeling and analyses outlined in the previous sections for the coastal region of China. Our results mainly include the wave height distribution along the coast corresponding to given return periods of 200, 500, 1000, and 2000 years, and the exposure and vulnerability index values of coastal cities. Subsequently, we map the different levels of tsunami hazard, exposure, vulnerability, and risk for the coastal cities.

4.1 Tsunami Hazard

At every hazard point along the coast, we calculated the wave height distribution corresponding to a given return period (Fig. 3). Tsunami wave heights are an increasing function of recurrence time and do not exceed 3 m in 200 years, 500 years, 1000 years, and 2000 years. As expected, as the return period increases, the wave height also increases, especially on the southeastern coast of the Bohai Sea and in the Yangtze River Delta and Pearl River Estuary.

The Bohai Sea: the potential tsunami sources contributing to the tsunami hazard along the coast of the Bohai Sea include several local faults located in the south. The tsunami wave height on the northern coast is less than 0.5 m for return periods between 200 and 2000 years. In comparison, the greatest wave height on the southern coast is higher than 0.5 m for 200 years and is close to 3 m for 2000 years. The cities where tsunami wave height values may be higher than 2.5 m are Qinhuangdao, Tangshan, and Yantai.

The East China Sea: the tsunami wave heights along the East China Sea are very unequally distributed, and the main sources come from the Ryukyu Trench and a local seismic source (Subei fault). The coast where wave heights are expected to be high is the Yangtze River Delta. The largest wave height is higher than 1 m for 200 years and is close to 3 m for 2000 years. The cities where tsunami wave height values may be higher than 2 m are Ningbo and Zhoushan.

The South China Sea: the coasts where tsunami wave heights are expected to be high are the Pearl River Estuary and areas near the Taiwan Strait. The largest wave height is higher than 0.5 m for 200 years and close to 3 m for 2000 years, and the main threats come from the Manila Trench and local seismic sources (the faults on the continental shelves). The cities where tsunami wave height values may be higher than 2.5 m include Hong Kong, Macao, Xiamen, and Quanzhou.

As shown in Fig. 4, most cities are at the low hazard level (level IV) for 200 years and at the medium–high hazard level (level II) for 2000 years. Specifically, Tangshan, Yantai, Hong Kong, and Macao are at the high hazard level (level I) for 2000 years.

4.2 Exposure to Tsunamis

Exposure is defined as the presence of people and of property that is prone to potential damage. As shown in Fig. 5a, the Bohai Sea rim, Yangtze River Delta, and Pearl River Delta are the areas with the highest exposure in the study region. These areas have flat landscape with low elevations, fertile soils, and convenient transportation, and

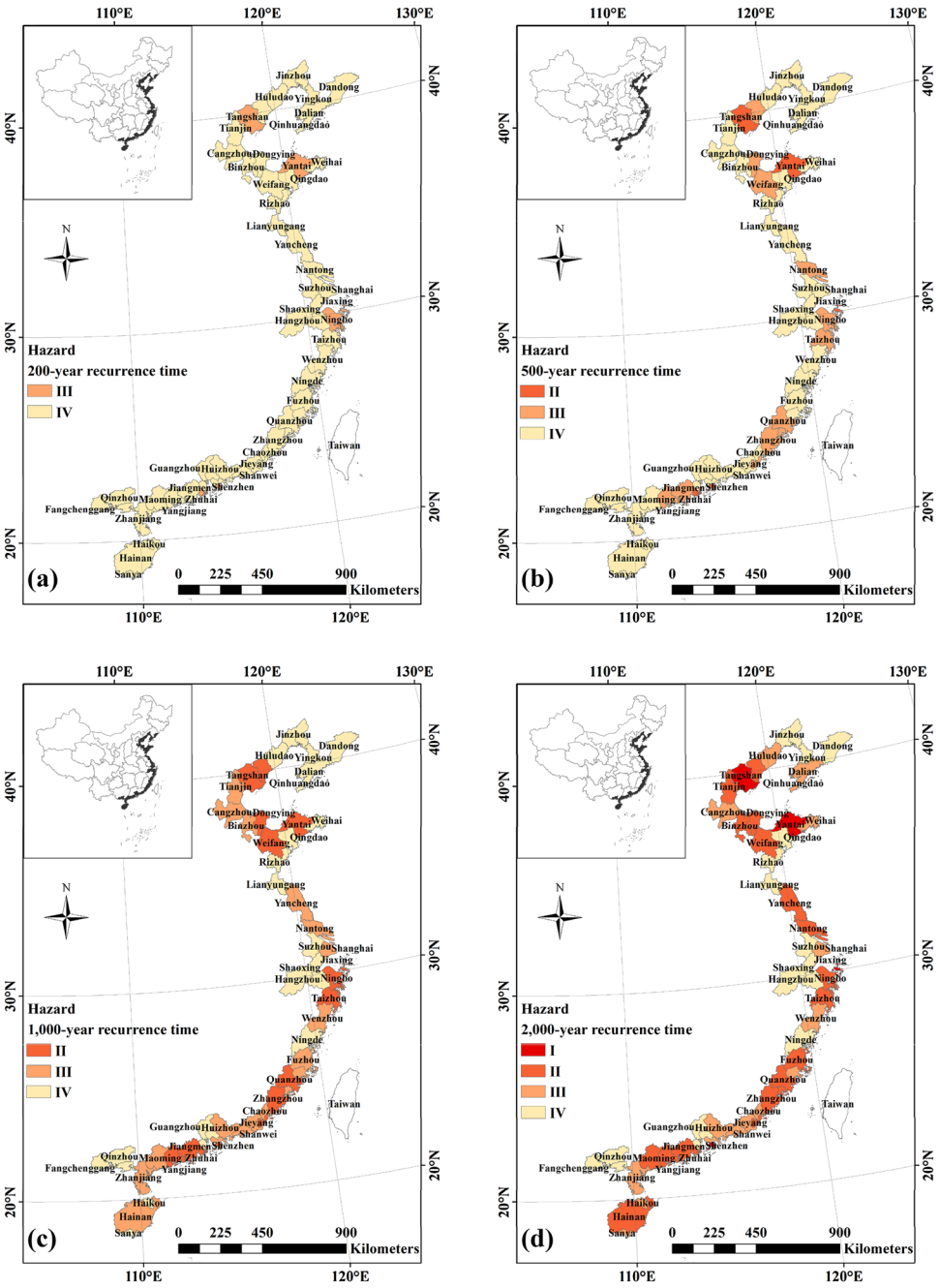

Fig. 4 Hazard level distributions in coastal cities of China for return periods of **a** 200 years, **b** 500 years, **c** 1000 years, and **d** 2000 years

most are areas where the economy and population are concentrated.

Specifically, Tianjin and Qingdao have high exposure to tsunamis on the Bohai Sea rim. The GDP of these two cities exceeds RMB 1 trillion yuan, and the population of each has reached nearly 10 million.[3] The Yangtze River Delta urban agglomerations also have a high level of exposure to tsunamis, especially in Shanghai, Hangzhou, Suzhou, and Ningbo, which have highly concentrated economic development and populations. In the Pearl River Delta region, the exposure is more concentrated, with Hong Kong, Guangzhou, and Shenzhen concentrating 22% of the GDP and 11% of the population in the region.[4]

4.3 Vulnerability to Tsunamis

Vulnerability is understood as the potential capacity of local socioeconomic systems to respond to tsunamis. As shown in Fig. 5b, the vulnerability map at the city level in coastal China was obtained from the vulnerability index,

[3] https://www.resdc.cn/..

[4] https://www.resdc.cn/

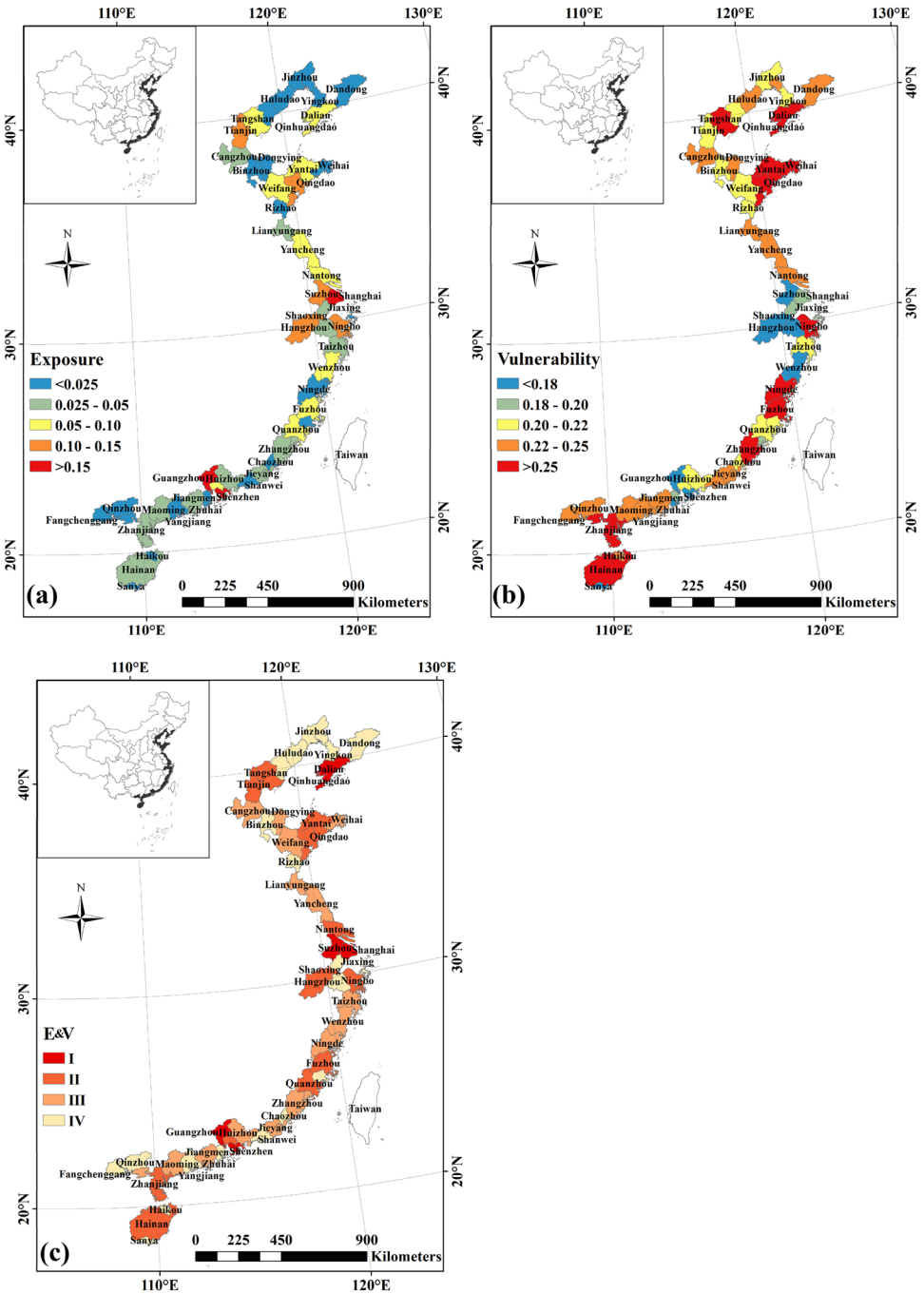

Fig. 5 Exposure and vulnerability index values and classification of disaster-prone areas in coastal cities of China. **a** Values of the exposure index, **b** values of the vulnerability index, and **c** classification of exposure and vulnerability

which was calculated using indicators related to vulnerability. This map shows that the areas with high vulnerability to tsunami along the Chinese coast are concentrated in the Bohai Sea rim, Shanghai, Fuzhou, and Hainan. In comparison, the vulnerabilities of Hangzhou, Shaoxing, Suzhou, and Guangzhou on the Yangtze River Delta are at relatively low levels of vulnerability due to the short coastline, advanced science and technology development, and higher fortification intensity.

4.4 Tsunami Risk

City-level hazard, exposure, and vulnerability to tsunamis are integrated to determine the risk level, and the spatial distribution of tsunami risk along the coast of China is illustrated in Fig. 6. The results show the tsunami risk at the city level according to the tsunami risk severity classes: high, medium–high, medium–low, and low. The spatial variations of the medium–high and high severity classes are much greater than those of the medium–low and low

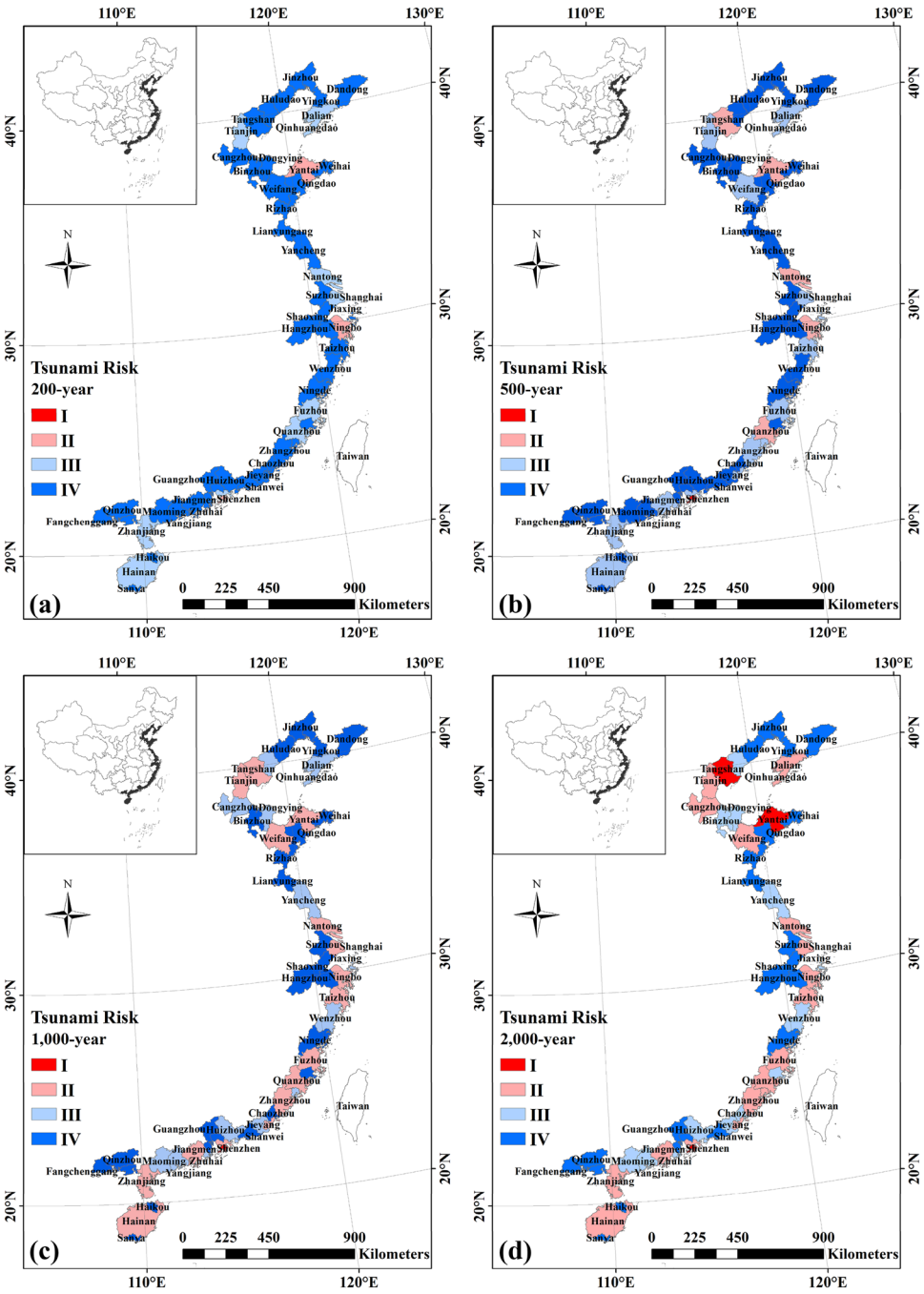

Fig. 6 Risk distributions in coastal cities of China for return periods of **a** 200 years, **b** 500 years, **c** 1000 years, and **d** 2000 years

tsunami risks. Cities in the northern part of the Bohai Sea rim, most of the cities on the eastern coast, and some of the cities on the southern coast are far away from tsunami sources, and their risk levels are medium–low and low. The medium–high and high levels of risk are found in the southern cities of the Bohai Sea, Yangtze River Delta, and Pearl River Estuary, which is partially related to the relatively dense population, urbanization, and economic development of these regions. Another important reason is that these cities are also closer to tsunami sources, for example, the coastal urban areas in Fujian Province on the western side of the Taiwan Strait.

As the return period increases, the number of cities with medium–high and high risk increases. Specifically, based on the difference between the 200-year wave height (Fig. 6a) and 500-year wave height (Fig. 6b), Hong Kong changed from medium–high risk (level II) to the high risk level (level I), and Yantai, Ningbo, Tangshan, Nantong, and Quanzhou present the medium–high risk level (level II). The 1000-year wave height (Fig. 6c) shows that more

cities are at the medium–high risk level (level II). Based on the difference between the 1000-year wave height (Fig. 6c) and 2000-year wave height (Fig. 6d), the cities at the high risk level (level I) include Tangshan, Yantai, Shanghai, and Hong Kong.

5 Discussion

Similar to many coastal countries and regions, China and its coastal cities may expect to face the threat of tsunamis in the future, which will adversely affect people, plants and animals, economic systems, assets, and so on. Against this background, the Ministry of Natural Resources recently developed the Guideline for Risk Assessment and Zoning of Tsunami Disaster (Ministry of Natural Resources 2019) with the aim of providing guidelines for proactive tsunami risk management. This study responded to those policy needs expressed in the Guideline and examined the spatial distribution of the tsunami risk for China's coastal cities. By integrating tsunami hazard information and indicators of the associated exposure and vulnerability, our analysis goes beyond existing studies, which have focused on either simulation-based hazard assessment (Ren et al. 2014; Ren et al. 2017; Yuan et al. 2021) or assessment of vulnerability to tsunamis (Batzakis et al. 2020).

Tsunami hazards can be described by the wave height distribution along the coast corresponding to a given return period. The wave heights of tsunamigenic earthquakes are subject to considerable uncertainty using the PTHA method (Selva et al. 2016; Davies et al. 2017; Yuan et al. 2021). Knowledge uncertainties can be decreased based on new insights. In this study, the characteristics and seismicity of the tsunami source zones along the Chinese coast are determined based on the latest research results (Ren et al. 2017; Xie et al. 2020). The Monte Carlo technique was applied to reduce the random uncertainties in the PTHA method. In addition, the analysis we performed included only tsunamis caused by earthquakes with Mw $\geq$ 7, which is considered the minimum magnitude at which a tsunami threat could occur in the waters off China's coast (Ren et al. 2014; Ren et al. 2017; Yuan et al. 2021). Inappropriate linear/nonlinear shallow wave propagation theory choices in numerical simulations may underestimate or overestimate hazards (Glimsdal et al. 2013; Yuan et al. 2021). For tsunamis generated in the Ryukyu Trench and Manila Trench, the tsunami wave amplitude is much smaller than the water depth; thus, the linear shallow wave propagation theory can be adopted. For tsunamis generated by local crustal faults on continental shelves, the nonlinear convective inertia force and bottom friction terms become increasingly prominent; therefore, nonlinear shallow wave propagation theory is a better choice.

A composite index is very effective for aggregating multiple potential exposure and vulnerability indicators, although using incomplete datasets has certain limitations (Sherbinin et al. 2019). There is no uniform or standard procedure for using indicators to measure exposure and vulnerability to tsunamis. However, indicators must address multiple dimensions that are highly relevant in the context of exposure and vulnerability. Some crucial indicators of exposure have been widely used and have gained consensus within the community, such as population and GDP (Dewan 2013; Batzakis et al. 2020). Vulnerability is a multidimensional construct, and we selected the indicators according to the perspectives of resilience and adaptability. Cities with high GDP per capita are characterized by higher levels of social development and industrialization. These features ensure that these cities are more resilient to tsunamis and may suffer fewer losses (Gao et al. 2020). Therefore, GPD per capita can also reflect a city's resilience level, as can natural factors, such as coastline length and average elevation. In the face of tsunami disasters, human capacity, which is the human ability to objectively understand the disaster and allocate and transport limited resources, is the key factor reflecting local adaptive capacity to tsunami disasters (Thorn et al. 2015). The proportion of social security personnel and the proportion of science and technology expenditure selected in this study can reflect a city's adaptability.

6 Conclusion

Tsunami risk assessment is one of the fundamental components of integrated management of natural hazard-related disasters in coastal cities. This article highlights a method of conducting such an assessment from an integrated perspective by emphasizing the combined role of hazard, exposure, and vulnerability to tsunamis. Our work may provide valuable information for future disaster management in coastal cities.

The PTHA shows that the tsunami wave heights are an increasing function of recurrence time in 200 years, 500 years, 1000 years, and 2000 years. As the return period increases, the wave height also increases. The composite index of exposure and vulnerability shows that the cities around the Bohai Sea rim, on the Pearl River Delta, and on the Yangtze River Estuary have the highest levels of exposure and vulnerability. The results of the tsunami risk assessments for all coastal cities in China's mainland show that the tsunami risk level is related to the recurrence time. The 200-year wave height implies that most cities are at the medium–low and low risk levels (levels III and IV). In comparison, the 2000-year wave height indicates that many cities are at the medium–high risk level (level II), while

Tangshan, Yantai, and Hong Kong are at the high risk level (level I).

This work presents a regional study of tsunami risk where one has to use coarse bathymetry, so there is no refined assessment of the inundation extent in small areas. Future studies can be based on the research method in this article to reduce the regional scale to specific cities. In this way, the wave height and inundation extent of tsunami disasters can be quantitatively evaluated, which is of practical significance for future urban planning. In addition, exposure and vulnerability assessment can be based on big data methods such as deep learning, which can be conducted in a temporally dynamic way and encourage coastal cities to shift from reactive to proactive tsunami risk management.

Acknowledgments This research was supported by the National Natural Science Foundation of China (Grant No. 41771537) and the Fundamental Research Funds for the Central Universities.

References

Aki, K. 1966. Generation and propagation of G waves from the Niigata Earthquake of June 16, 1964: Part 2. Estimation of earthquake moment, released energy and stress drop from the G wave spectra. *Bulletin of the Earthquake Research Institute, University of Tokyo* 44(1): 73–88.

Ambraseys, N., and C. Synolakis. 2010. Tsunami catalogs for the Eastern Mediterranean, revisited. *Journal of Earthquake Engineering* 14(3): 309–330.

Batzakis, D.V., L.M. Misthos, G. Voulgaris, K. Tsanakas, and E. Karymbalis. 2020. Assessment of building vulnerability to tsunami hazard in Kamari (Santorini Island, Greece). *Journal of Marine Science and Engineering* 8(11): Article 886.

Choi, B.H., B.I. Min, T. Yoshinobu, K.O. Kim, and E. Pelinovsky. 2012. Comparable analysis of the distribution functions of runup heights of the 1896, 1933 and 2011 Japanese Tsunamis in the Sanriku area. *Natural Hazards & Earth System Sciences* 12(5): 1463–1467.

Cong, L., M. Gao, G. Wu, and X. Wu. 2019. The concentration of population and GDP in high earthquake risk regions in China: Temporal–spatial distributions and regional comparisons from 2000 to 2010. *Pure and Applied Geophysics* 176(10): 4161–4175.

Cornell, C.A. 1968. Engineering seismic risk analysis. *Bulletin of Seismological Society of America* 58(5): 1583–1606.

Davies, G., J. Griffin, F. Lovholt, S. Glimsdal, C. Harbitz, H.K. Thio, S. Lorito, and R. Basili et al. 2017. A global probabilistic tsunami hazard assessment from earthquake sources. *Geological Society, London, Special Publications* 456(1): 219–244.

De Risi, R., K. Goda, N. Mori, and T. Yasuda. 2017. Bayesian tsunami fragility modeling considering input data uncertainty. *Stochastic Environmental Research and Risk Assessment* 31(5): 1253–1269.

Dewan, A.M. 2013. Spatial and temporal distribution of floods. In *Floods in a megacity: Geospatial techniques in assessing hazards, risk and vulnerability*, ed. A. Dewan, 103–127. Heidelberg: Springer.

Feng, X., B. Yin, S. Gao, P. Wang, T. Bai, and D. Yang. 2017. Assessment of tsunami hazard for coastal areas of Shandong Province, China. *Applied Ocean Research* 62: 37–48.

Field, C.B., V. Barros, J. Dokken, K.J. Mach, M.D. Mastrandrea, T.E. Bilir, M. Chaterjee, and L. Ebi et al. eds. 2014. In *Climate change 2014—Impacts, adaptation, and vulnerability. Part A: Global and sectoral aspects. Contribution of Working Group II to the Fifth Assessment Report of the Intergovernmental Panel on Climate Change*. Cambridge, UK: Cambridge University Press.

Frischen, J., I. Meza, D. Rupp, K. Wietler, and M. Hagenloche. 2020. Drought risk to agricultural systems in Zimbabwe: A spatial analysis of hazard, exposure, and vulnerability. *Sustainability* 12(3): Article 752.

Gao, Z., M. Ding, T. Huang, and X. Hu. 2020. Geohazard vulnerability assessment in Qiaojia seismic zones, SW China. *International Journal of Disaster Risk Reduction* 52: Article 101928.

Geist, E.L., and T. Parsons. 2006. Probabilistic analysis of tsunami hazards. *Natural Hazards* 37(3): 277–314.

Glimsdal, S., G.K. Pedersen, C.B. Harbitz, and F. Løvholt. 2013. Dispersion of tsunamis: Does it really matter?. *Natural Hazards and Earth System Sciences* 13(6): 1507–1526.

Goto, K., T. Kawana, and F. Imamura. 2010. Historical and geological evidence of boulders deposited by tsunamis, southern Ryukyu Islands, Japan. *Earth Science Reviews* 102(1–2): 77–99.

Grezio, A., A. Babeyko, M.A. Baptista, J. Behrens, A. Costa, G. Davies, E.L. Geist, and S. Glimsdal et al. 2017. Probabilistic tsunami hazard analysis: Multiple sources and global applications. *Reviews of Geophysics* 55(4): 1158–1198.

Harbitz, C.B., S. Glimsdal, S. Bazin, N. Zamora, F. Løvholt, H. Bungum, H. Smebye, P. Gauer, and O. Kjekstad. 2012. Tsunami hazard in the Caribbean: Regional exposure derived from credible worst case scenarios. *Continental Shelf Research* 38: 1–23.

Hou, J.M., X.J. Li, Y. Yuan, and P.T. Wang. 2016. Tsunami hazard assessment along the Chinese mainland coast from earthquakes in the Taiwan region. *Natural Hazards* 81(2): 1269–1281.

Hu, Q.L., Z.C. Dong, Y.F. Yang, B. Li, and J.T. Zhang. 2019. State evaluation model of water resources carrying capacity based on connection number. *Journal of Hohai University (Natural Sciences)* 47(5): 425–432.

Huang, G.R., H.W. Luo, X.X. Lu, C.H. Yang, Z. Wang, T. Huang, and J.G. Ma. 2020. Study on risk analysis and zoning method of urban flood disaster. *Water Resources Protection* 36(6): 1–7.

Huang, Z., T.R. Wu, S.K. Tan, K. Megawati, F. Shaw, X. Liu, and T.C. Pan. 2009. Tsunami hazard from the subduction megathrust of the South China Sea: Part II. Hydrodynamic modeling and possible impact on Singapore. *Journal of Asian Earth Sciences* 36(1): 93–97.

Kaistrenko, V. 2011. Tsunami recurrence versus tsunami height distribution along the coast. *Pure and Applied Geophysics* 168(11): 2065–2069.

Li, H.W., Z.C. Wang, Y. Yuan, Z.G. Xu, P.T. Wang, and J.Y. Shi. 2019. Probabilistic tsunami hazard assessment in the Bohai Sea. *Haiyang Xuebao* 41(1): 51–57 (in Chinese).

Li, L., A. Switzer, C.H. Chan, Y. Wang, R. Weiss, and Q. Qiu. 2016. How heterogeneous coseismic slip affects regional probabilistic tsunami hazard assessment: A case study in the South China Sea. *Journal of Geophysical Research Solid Earth* 121(8): 6250–6272.

Li, X.M., and P.Y. Jin. 2012. Characteristics and spatial–temporal differences of urban human settlement environment in China. *Scientia Geographica Sinica* 32(5): 521–529.

Liu, L.F., X. Wang, and A.J. Salisbury. 2009. Tsunami hazard and early warning system in South China Sea. *Journal of Asian Earth Sciences* 36(1): 2–12.

Liu, Y.C., A. Santos, S.M. Wang, Y.L. Shi, H.L. Liu, and D.A. Yuen. 2007. Tsunami hazards along Chinese coast from potential earthquakes in South China Sea. *Physics of the Earth and Planetary Interiors* 163(1): 233–244.

Lorito, S., M.M. Tiberti, R. Basili, A. Piatanesi, and G. Valensise. 2008. Earthquake-generated tsunamis in the Mediterranean Sea: Scenarios of potential threats to Southern Italy. *Journal of Geophysical Research Solid Earth* 113(B1): Article B01301.

Løvholt, F., S. Glimsdal, C.B. Harbitz, N. Horspool, H. Smebye, A. de Bono, and F. Nadim. 2014. Global tsunami hazard and exposure due to large co-seismic slip. *International Journal of Disaster Risk Reduction* 10(Part B): 406–418.

Ministry of Natural Resources. 2019. Guideline for risk assessment and zoning of tsunami disaster. Beijing: State Oceanic Administration of China (in Chinese).

Mori, N., K. Goda, and D. Cox. 2018. Recent process in Probabilistic Tsunami Hazard Analysis (PTHA) for mega thrust subduction earthquakes. In *The 2011 Japan Earthquake and Tsunami: Reconstruction and restoration*, ed. V. Santiago-Fandiño, S. Sato, N. Maki, and K. Iuchi, 469–485. Cham: Springer.

Nan, Y., J. Ji, H.D. Feng, and C.C. Zhang. 2013. On eco-security evaluation in the Tumen River region based on RS&GIS. *Acta Ecologica Sinica* 33(15): 4790–4798.

Ning, L.X., C.X. Cheng, A.M. Cruz, and E. Garnier. 2021. Exploring of the spatially varying completeness of a tsunami catalogue. *Natural Hazards*. https://doi.org/10.1007/s11069-021-05049-1.

Ömer, A., and T. Naohiko. 2019. Tsunami boulders and their implications on the potential for a mega-earthquake along the Ryukyu Archipelago, Japan. *Bulletin of Engineering Geology and the Environment* 78(6): 3917–3925.

Omira, R., M.A. Baptista, and L. Matias. 2015. Probabilistic tsunami hazard in the Northeast Atlantic from near- and far-field tectonic sources. *Pure and Applied Geophysics* 172(3): 901–920.

Okada, Y. 1985. Surface deformation due to shear and tensile faults in a half-space. *Bulletin of the Seismological Society of America* 75(4): 1135–1154.

Ortega-Gaucin, D., J.A. Ceballos-Tavares, A. Ordoñez Sánchez, and H.V. Castellano-Bahena. 2021. Agricultural drought risk assessment: A spatial analysis of hazard, exposure, and vulnerability in Zacatecas, Mexico. *Water* 13(10): Article 1431.

Pan, H., M.T. Gao, and F.R. Xie. 2013. The earthquake activity model and seismicity parameters in the new seismic hazard map of China. *Technology for Earthquake Disaster Prevention* 8(1): 11–23.

Papazachos, B.C., E.M. Scordilis, D.G. Panagiotopoulos, C.B. Papazachos, and G.F. Karakaisis. 2004. Global relations between seismic fault parameters and moment magnitude of earthquakes. *Bulletin of the Geological Society of Greece* 36(3): 1482–1489.

Parsons, T., and E.L. Geist. 2008. Tsunami probability in the Caribbean region. *Pure and Applied Geophysics* 165(11): 2089–2116.

Philip, F.L., S.B. Woo, and Y.C. Cho. 1998. Computer programs for tsunami propagation and inundation. Technical report. Cornell University, Ithaca, NY, USA.

Power, W., X. Wang, E. Lane, and P. Gillibrand. 2013. A probabilistic tsunami hazard study of the Auckland region, Part I: Propagation modelling and tsunami hazard assessment at the shoreline. *Pure and Applied Geophysics* 170(9): 1621–1634.

Ren, L.C., Y. Xue, C.L. Jian, and W. Feng. 2009. Sensitivity analysis of the effect of the earthquake magnitude in potential tsunami source on the tsunami wave amplitude in the northern area of the South China Sea. *Earthquake Research in China* 25(2): 186–192.

Ren, Y., R. Wen, and Y. Song. 2014. Recent progress of tsunami hazard mitigation in China. *Episodes* 37(4): 277–283.

Ren, Y., R. Wen, P. Zhang, Z. Yang, R. Pan, and X. Li. 2017. Implications of local sources to probabilistic tsunami hazard analysis in South Chinese coastal area. *Journal of Earthquake & Tsunami* 11(1): Article 1740001.

Selva, J., R. Tonini, I. Molinari, M.M. Tiberti, F. Romano, A. Grezio, D. Melini, and A. Piatanesi et al. 2016. Quantification of source uncertainties in Seismic Probabilistic Tsunami Hazard Analysis (SPTHA). *Geophysical Journal International* 205(3): 1780–1803.

Shaw, B., N.N. Ambraseys, P.C. England, M.A. Floyd, G.J. Gorman, T. Higham, J.A. Jackson, and J.M. Nocquet et al. 2008. Eastern Mediterranean tectonics and tsunami hazard inferred from the AD 365 earthquake. *Nature Geoscience* 1(4): 268–276.

Sherbinin, A. de., A. Bukvic, G. Rohat, M. Gall, B. McCusker, B. Preston, A. Apotsos, C. Fish, et al. 2019. Climate vulnerability mapping: A systematic review and future prospects. *Wiley Interdisciplinary Reviews: Climate Change* 10(5): Article e600.

Shen, S., C.X. Cheng, C.Q. Song, J. Yang, S.L. Yang, K. Su, L.H. Yuan, and X.Q. Chen. 2018. Spatial distribution patterns of global natural disasters based on biclustering. *Natural Hazards* 92(3): 1809–1820.

Shi, P.J. 1996. Theory and practice of disaster study. *Journal of Natural Disasters* 5(4): 6–17 (in Chinese).

Shi, F., L.S. Bi, X.B. Tan, Z.Y. Wei, and H.L. He. 2012. Did earthquake tsunami occur in Bohai Sea in history?. *Chinese Journal of Geophysics Chinese Edition* 55(9): 3097–3104 (in Chinese).

Smit, A., A. Kijko, and A. Stein. 2017. Probabilistic tsunami hazard assessment from incomplete and uncertain historical catalogues with application to tsunamigenic regions in the Pacific Ocean. *Pure and Applied Geophysics* 174(8): 3065–3081.

Thorn, J., T.F. Thornton, and A. Helfgott. 2015. Autonomous adaptation to global environmental change in peri-urban settlements: Evidence of a growing culture of innovation and revitalisation in Mathare Valley Slums, Nairobi. *Global Environmental Change* 31: 121–131.

UNISDR (United Nations Office for Disaster Risk Reduction). 2019. *Global assessment report on disaster risk reduction 2019*. Geneva: United Nations.

Wang, G., Y. Liu, Z. Hu, Y. Lyu, G. Zhang, J. Liu, Y. Liu, Y. Gu, et al. 2020. Flood risk assessment based on fuzzy synthetic evaluation method in the Beijing–Tianjin–Hebei metropolitan area, China. *Sustainability* 12(4): Article 1451.

Wang, P., G. Yi, F. Yu, and T. Fan. 2014. Quantitative research on earthquake-generated tsunami hazards based on the numerical simulations in Bohai Sea. *Acta Oceanologica Sinica* 36(1): 56–64.

Wijetunge, J.J. 2014. A deterministic analysis of tsunami hazard and risk for the southwest coast of Sri Lanka. *Continental Shelf Research* 79: 23–35.

Witter, R.C., H.M. Kelsey, and E. Hemphill-Haley. 2003. Great Cascadia earthquakes and tsunamis of the past 6700 years,

Coquille River Estuary, southern coastal Oregon. *Geological Society of America Bulletin* 115(10): 1289–1306.

Wu, T.R., and H.C. Huang. 2009. Modeling tsunami hazards from Manila Trench to Taiwan. *Journal of Asian Earth Sciences* 36(1): 21–28.

Xie, Z., S.Y. Li, Y.J. Lv, W.J. Xu, Y.L. Zhang, and W.X. Liu. 2020. Unified earthquake catalog for China's Seas and adjacent regions and its completeness analysis. *Seismology and Geology* 42(4): 993–1019 (in Chinese).

Ye, T., W. Liu, Q. Mu, S. Zong, Y. Li, and P. Shi. 2020. Quantifying livestock vulnerability to snow disasters in the Tibetan Plateau: Comparing different modeling techniques for prediction. *International Journal of Disaster Risk Reduction* 48: Article 101578.

Yuan, Y., H. Li, Y. Wei, F. Shi, and Z. Xu. 2021. Probabilistic Tsunami Hazard Assessment (PTHA) for southeast coast of Chinese Mainland and Taiwan Island. *Journal of Geophysical Research Solid Earth* 126(2): Article e2020JB020344.

Zamora, N., and A.Y. Babeyko. 2020. Probabilistic tsunami hazard assessment for local and regional seismic sources along the Pacific Coast of Central America with emphasis on the role of selected uncertainties. *Pure and Applied Geophysics* 177(3): 1471–1495.

Zhang, X., J. Song, J. Peng, and J. Wu. 2019. Landslides-oriented urban disaster resilience assessment—A case study in Shenzhen, China. *Science of the Total Environment* 661: 95–106.

Zhou, C., M. Chang, L. Xu, and H.X. Che. 2020. Risk assessment of typical urban mine geological disasters in Guizhou Province. *Geomatics and Information Science of Wuhan University* 45(11): 1782–1791 (in Chinese).

Zhou, Q., and W.M. Adams. 1988. Tsunami risk analysis for China. *Natural Hazard* 1(2): 181–195.